Experience with Aero- and Fluid-Dynamic Testing for Engineering and CFD Validation

James C. Ross
NASA Ames Research Center
Mail Stop 260-1
Moffett Field, CA 94035
USA

james.c.ross@nasa.gov

ABSTRACT

Ever since computations have been used to simulate aerodynamics the need to ensure that the computations adequately represent real life has followed. Many experiments have been performed specifically for validation and as computational methods have improved, so have the validation experiments. Validation is also a moving target because computational methods improve requiring validation for the new aspect of flow physics that the computations aim to capture. Concurrently, new measurement techniques are being developed that can help capture more detailed flow features – pressure sensitive paint (PSP) and particle image velocimetry (PIV) come to mind. This paper will present various wind-tunnel tests the author has been involved with and how they were used for validation of various kinds of CFD. A particular focus is the application of advanced measurement techniques to flow fields (and geometries) that had proven to be difficult to predict computationally. Many of these difficult flow problems arose from engineering and development problems that needed to be solved for a particular vehicle or research program. In some cases the experiments required to solve the engineering problems were refined to provide valuable CFD validation data in addition to the primary engineering data. All of these experiments have provided physical insight and validation data for a wide range of aerodynamic and acoustic phenomena for vehicles ranging from tractor-trailers to crewed spacecraft.

1.0 INTRODUCTION

Ever since starting work at NASA doing wind tunnel testing, the death of wind tunnels by CFD has been 10 to 20 years off. Luckily for me the CFD community has needed more and more validation experiments in order

to bring about such a demise. It wasn't until very recently that I made the connection that nearly all of the tests I've run or been associated with have involved at least some aspect of validation or verification. From panel codes for phenomena like fuselage lift carryover, to Navier-Stokes codes requiring detailed unsteady measurements for bluff-body aerodynamics, there is a seemingly endless need for data to ensure that we aren't being mislead by the ever improving and very impressive computations that we are capable of.

Validation and verification of CFD has been discussed at length in the technical literature. I will be talking specifically about providing data for validation, defined as "The process of determining the degree to which a model is an accurate representation of the real world from the perspective of the intended uses of the model" [1]. The other aspect of testing for CFD that I'll talk about is calibration, by which I mean developing an understanding of how to generate and interpret computational results for a given configuration and relatively small variations thereof. This is a particularly useful exercise for the development of an aerodynamic database for a flight vehicle and is a distinct and perhaps more limited sort of validation than is generally considered, but is nevertheless very commonly done.

I will present a loose chronology of testing I've been involved with and a discussion about how CFD benefitted (usually, but not always by intent) and how the projects have combined CFD and experiments to maximize the understanding of particular configurations and flow phenomena. Many of the projects were primarily research but generally with a particular application in mind or as an end goal. Others have been more development projects for either aeronautics or space applications - either launch or reentry aerodynamics/aeroacoustics. I'll close with two more basic research projects and some thoughts about where I see the next big payoffs in validation/verification testing might be. The central message is that there is a sufficient level of complexity of experiment or measurement technique appropriate for a given flow and computational tool. In a research environment it is perfectly acceptable to simply go all out on an experiment and let the codes and CFD practitioners catch up. In a development project, there is more value placed on time and cost so the experiments to validate the CFD tools being used must be more focused and specific.

2.0 POTENTIAL FLOW VALIDATION

2.1 Wing-Fuselage Interference

In the early 1980's, the state of CFD was much less advanced than today but we still needed to use the available methods to help design and analyze aircraft. My early experience with CFD was incompressible potential flow panel codes. I was assigned to study wing-fuselage interference and the tool available was a panel code, VSAERO [2, 3]. These computational tools may seem a bit dated but still have their place for rapid design analyses and quick looks at subsonic flow situations with little or no flow separation. For wing-fuselage interference there was limited data available – a very systematic German study of wing position on simple-shaped fuselage shapes[4-6] and some full-scale data on a Beech Sundowner in the 40x80 Foot Wind Tunnel at NASA Ames Research Center[7]. Even this relatively low-fidelity data was useful for "tuning" VSAERO to match lift distributions and pressure signatures. It did little to advance the strictly predictive capability of the code but helped form guidance for the code user to model the viscous effects present on specific aircraft configurations the the expected lift carried by the fuselage. Figures 1 and 2 show some of the matches obtained using VSAERO.

The result of this study led to a better understanding of the important parameters to adjust in the panel code to better simulate lift carry over. The primary factor was carrying the proper percentage of lift across the fuselage, primarily by shedding the correct amount of vorticity at the wing root and properly placing the wake cut along the aft part of the fuselage. The lessons learned from the Sundowner testing led to new features in the code to facilitate the correct modeling of carryover lift. VSAERO and a similar code, PMARC[8] are still in common use and have incorporated the lessons from the data in these two studies (and of course many more) to increase the automation and accuracy of cases run using them. Even though the experiments were not designed from a validation perspective, both have had a significant effect on the ability of engineers today to model substantially attached-flow subsonic vehicles.

2.2 Wind Tunnel Inlet Design

A subsequent use of potential flow analysis was to design the inlet shape and inlet vanes for the 80- by 120-Foot Wind Tunnel[9, 10]. Figure 2-3 is photograph showing the wind-tunnel inlet. The goal was to design the inlet and turbulence-reduction treatment to provide less than 0.5% variation in dynamic pressure across the center 75% of the test section and less than 0.5% turbulence intensity. We used 2-dimensional potential flow codes to tailor the vane angles to manipulate the inflow so that the pressure drop through the screens was uniform across the full 1.03 acres of inlet area. Computers being what they were in those days, the analysis of the inlet and the 120 vanes was done in two dimensions. The panel code HILIFT[11] gave the inlet flow velocity and the angle of the flow relative to the screen normal from which the pressure drop was computed. The three-dimensionality of the flow was sufficient to make this only an approximate answer. The approach was then to optimize the vane angles in two dimensions, test the configuration in a $1/15^{th}$-scale model of the wind tunnel. The difference between the predicted and measured dynamic pressure distributions was used as a correction factor for a subsequent round of optimization. The process converged and we came up with a configuration that met the flow uniformity criterion and the sub-scale wind tunnel proved that the test section turbulence was acceptable.

This process isn't what one would normally think of as CFD validation but it was critical for this project. It is probably best called a calibration activity. Without it, the design would have been much more time consuming – mounting the inlet vanes in the sub-scale wind tunnel was tedious and the CFD in the loop probably reduced the number of configurations tested by at least a factor of 10. These kinds of tests that provide problem specific verification of computational tools are extremely useful and have been a big part of both research and development projects that I've participated in. The kinds of data collected can be rather limited as long as there is sufficient information to provide clear trends for the CFD to capture and the user to interpret.

3.0 NAVIER-STOKES CODE VALIDATION

3.1 High-Lift Aerodynamics

One of my early steps in studying the three-dimensional flow over high-lift systems was a relatively simple unswept wing with a part-span flap[12-14]. The configuration is shown in Figure 3-1. While it is a very simplified geometry relative to an actual aircraft, some important features are present; a representative flap gap and overlap, the flap tip, and the change in the main element geometry at the end of the flap. Blowing slots on the end plates helped to approximate a slip condition on those surfaces to further reduce the flow complexity for the companion computations. The test was planned as a validation case for the INS3D-UP (incompressible Navier-Stokes upwind differenced) code. The structured, overset grids used in this code were used to an advantage in that the transitions from one portion of the model to the next could be abrupt which meant the various parts could be built as “extrusions” with squared off ends that were exactly matched in the CFD surface grids. The details of the flow around the flap tip were of particular interest in this project because of the implications to airframe noise. The flap tip was instrumented with tightly spaced pressure taps. In order to get more details about the flow, we were able to try out the then new technique of pressure sensitive paint (PSP). The PSP was only marginally successful in this instance, but gave us a glimpse at the flow structure and gave hints at how the flap-tip vortex might be generating noise.

The development of new and more capable measurement techniques has generally led to better validation data sets for CFD. PSP is one but prior to that the move from the old mechanically-scanned pressure devices to electronically scanned pressure modules made it possible to measure pressures at a large number of locations on a model without spending inordinate amounts of wind-tunnel test time. 2000 pressure taps was an impressive number of taps in the 1990’s but PSP has increased that density of coverage to tens of thousands or more on a typical model. Off-body measurements also add to both the understanding of flow fields and to the CFD validation effort by providing additional clues about what flow features are being captured accurately or not.

The high-lift validation experiment was repeated twice more to cover additional geometry variations and to

measure the noise generated by the various aerodynamic elements. Figure 3-2 shows a flap and slat arrangement tested[15]. There were a large number of flap and slat deflection angles tested. The slat was tested full span and 0.75 span with the exposed tip on the un-flapped side of the model to make sure we could differentiate between the noise from the slat gap and the slat tip. A microphone array was installed in the wind-tunnel wall that provided the noise source locations as a function of frequency. At the time, unsteady flow, particularly at acoustic frequencies, was well beyond the capability of CFD to predict. The intent of the noise measurements was to find ways to reduce the different sources while the aerodynamic measurements were used to understand the noise measurements in the context of a flying aircraft as well as for CFD validation.

Figure 3-3 shows Particle Image Velocimetry (PIV) measurements in the slat cove region, which were an important aspect of the test and provided the biggest increment to the validation data from this series of tests. The measurements gave us mean velocity as well as turbulence quantities that helped tremendously in validating the CFD modeling. This particular set of experiments was a productive combination of CFD validation for the time-averaged pressures/aerodynamics[14] and an engineering study of ways to reduce airframe noise. It proved to be a cost effective test, and given the state of CFD for high-lift aerodynamics at the time, provided data with the right level of detail for validation. The core of the model was originally built almost 10 year prior to these tests to validate two-dimensional CFD for various hinged and slotted flap configurations (coupled potential-flow/boundary-layer analyses and Navier-Stokes), making the test even more cost-effective.

3.2 Class-8 Truck Drag

A very interesting and fruitful diversion from aircraft aerodynamics, the drag of class-8 trucks, provided a different perspective on both aerodynamics and CFD. The U.S. Department of Energy has been studying ways to reduce road vehicle drag for many years[16]. It is an ongoing effort that has always been a strong collaboration between experimentalists and CFD practitioners from government labs, universities, and industry. The early CFD work in the program concentrated on so-called time averaged, Reynolds Averaged

Navier-Stokes (RANS) codes. Comparisons between the wind tunnel results and the CFD quickly led to the realization that time averaged often meant non-time accurate in the CFD world, which are far from the same thing for unsteady flow fields. Bluff-body aerodynamics necessarily involves unsteady flows that have a loosely periodic nature and proper modeling requires time-accurate computations even if the interest is in the time-averaged results. As a result, most of the experiments gathered at least some unsteady information with the most interesting data coming from PIV measurements in the wake and in the gap between the tractor and trailer of a generic truck model[17] (Figures 3-4 and 3-5). Figure 3-4 shows the flow in the tractor/trailer gap with and without side extenders on the tractor which serve to partially block the flow through the gap in cross winds (thereby reducing the vehicle drag). In this case the extenders were made from optical-quality glass to enable the PIV measurements when they were installed. Also shown are the pressure distributions recorded at ~48 points on the back of the tractor and front of the trailer. The velocity color contours are the time-averaged vertical component of the flow in the measurement plane while the streamlines show the mean in-plane flow pattern.

A similar measurement in the wake of the trailer is shown in Figure 3-5. In this case the effect of angled boat-tail plates is documented. The plates are sized and positioned to provide some pressure recovery to the flow over the trailer before it separates into the wake. The result is reduced drag and a smaller wake.

Because of the very unsteady flow around truck shapes, the CFD used had to be time accurate leading to improved CFD capabilities in industry, universities, and government labs. The collaboration between the CFD researchers and the experimentalists in this project resulted in more rapid improvements in both areas than could have happened otherwise. Working together on the broader research program and planning, not just an individual test. resulted in more productive improvements in processes than typically result from validation experiments. This is likely because we developed a better understanding of the overall problem, the capabilities of the CFD and experimental methods, and what the specific problem areas were for truck aerodynamics.

3.3 Launch Vehicle and Spacecraft Aerodynamics

Another interesting diversion from aircraft aerodynamics was helping to develop the aerodynamic and aeroacoustic/buffet databases for the Orion spacecraft and the Space Launch System (SLS) launch vehicle. These two vehicles are key to the next generation of NASA human space exploration. I was mostly involved with wind-tunnel testing for the Orion Project. From the outset, the testing was intended to validate the CFD methods that were intended to be the basis of the aerodynamic database. As we got more into the project it became clear that the CFD tools, having been well validated for transonic cruise (and somewhat for high-lift aerodynamics) of transport aircraft, were not doing a good job with the bluff-body flows associated with capsules. For the capsule during descent, the disagreement between wind tunnel data and the CFD was primarily below Mach 2 and was particularly notable below Mach 1. The fraction of subsonic flight time during decent is small and mostly vertical and therefore doesn't affect the touchdown point. Of more concern was developing an accurate database for potential launch aborts where controllability and separation from a failing launch vehicle was critical. Early in the development of Orion, the launch vehicle was to be the Ares I which produced a very high dynamic pressure just as the vehicle was going transonic. The combination of high dynamic pressure at Mach 1 put pressure on the aero team to get the right answers.

Figure 3-6 shows the two aerodynamic configurations of the Orion for which aerodynamic databases were necessary. The Launch Abort Vehicle (LAV) was the most difficult to model because of the interactions between the various rocket plumes - Attitude Control Motor (ACM) used to steer the vehicle and Abort Motor (AM) which accelerate the LAV away from the launch vehicle at up to 10 g - and the vehicle surface. Figure 3-7 is a photograph taken just after initiation of a pad abort test of the Orion that shows both the AM and ACM plumes. The close interaction of the AM plumes and the LAV surface is readily apparent.

Modeling the plumes was a difficult problem for both CFD and wind tunnel testing. The initial testing included only the AM based on the seemingly sound assessment that the AM thrust is more than ten times the ACM thrust and would dominate the flow field. The images from the pad abort test flight seem to justify this assumption. The wind-tunnel testing was done with cold, high pressure air simulating the AM plumes with

consideration to the pressure and momentum ratio to approximate the nozzle exit Mach number and plume trajectory for expected flight conditions.

The CFD results for the wind-tunnel conditions were acceptably close to the measured results in many cases but subsequent analyses that included both the AM and ACM plumes showed surprisingly large interactions between the two sets of plumes. In some cases the control moments that the ACM should have provided (net thrust times the distance to the center of gravity) appeared to be reduced to near zero by the non-linear interactions with the AM plumes and their subsequent interactions with the LAV. Further adding to the uncertainty, computations intended to extrapolate the wind-tunnel results to flight conditions showed large changes in AM-plume-only interactions with the LAV due to differences in fluid characteristics between high-pressure air and the solid rocket plume (different chemical constituents and high-temperature). These two results led to two more wind tunnel tests to sort out the modeling problems in both the experiment and the CFD.

3.3.1 Abort Motor Plume Temperature Effects

The first test was a dedicated CFD validation test to examine the effect of plume temperature on the behavior of the AM plumes. After a long search for ways to heat the plume flow in a manner acceptable to managers at the wind tunnels that could provide the necessary optical access for PIV and high enough free-stream velocity we designed a test for the High Flow Jet Exit Rig at NASA's Glenn Research Center[19]. This facility provided 450 psi air at 1460 R to a single nozzle angled 25° or 40° relative to the Mach 0.3 surrounding flow. A model representative of the Orion LAV could be mounted downstream of the nozzle at the appropriate position. A three-component PIV system was used to measure the velocity in the plume either in isolation or with the LAV model. Figure 2-9 shows the test setup with the LAV model in place. The plume was run both cold and hot. Figure 2-10 shows PIV measurements of the plume velocity in a plane bisecting the nozzle and plume. While higher plume temperatures would have been better, these data enabled significant improvements in the high-temperature plume simulations. Keeping the experiment close to the "real" case increased the confidence in the database that was eventually populated with CFD-generated results.

3.3.2 Attitude-Abort Motor Plume Interactions

The second test used to sort out modeling issues with the abort motors included both the AM and ACM plumes. The ACM provides steering for the LAV by modulating the thrust from each of the 8 nozzles at the nose of the LAV. Figure 2-11 shows a section through the nozzles High pressure air was again chosen for the experiment but more care was taken to match the plume characteristics for both sets of nozzles because the experimental data was no longer primarily for CFD validate but might have been the only source for the aerodynamic database[20]. CFD played a big part in the plume matching in this case. The more traditional approach matched parameters like the ratio of the jet-exit and free-stream momentum with corrections for differences in the ratio of specific heats between the high-pressure air and solid rocket plume constituents. With this as a starting point, the model nozzle geometry was modified in CFD to match the desired exit conditions as well as the plume expansion seen in the computations of the flight plumes. This extra step made a noticeable difference, particularly because the AM plumes interact directly with the LAV and plume expansion directly affects the size of the plume interaction.

Designing a model to pass two independent high-pressure air supplies across a force and moment balance was another challenge requiring significant development work on high-pressure bellows and assembly in the model. The resulting model is shown in Figure 2-13 mounted in the wind tunnel. The CAD image below the photograph shows the various model components. The Service Module (SM) was included during part of the test to represent the launch vehicle during the initial separation of the LAV from the launch vehicle during an abort - a particularly important time to understand the drag of the LAV (or more properly the net thrust of the LAV). The SM model was mounted to a traverse allowing aft translation, vertical motion, and pitch changes. This model allowed rapid configuration changes for the separation simulation and changes to the thrust levels of the AM and ACM via the high-pressure-air system. Adjustments to the ACM firing direction and maximum thrust, however, required physically changing one or more of the 8 nozzles.

Figure 2-14 shows surface pressure maps on the LAV obtained using PSP[18]. PSP provided an extremely dense set of pressure data that was helpful in tracking trends with plumes on and off - as in these images. It also

helps in making comparisons between measured and computed results, particularly where pressure taps could not be installed (e.g. on the tower above and below the AM nozzles). Pressure changes in these areas can produce large moments about the center of gravity which is well aft so it is critical for the computations to get the right answers there. As a side benefit for working collaboratively with the CFD team, the PSP measured pressure distributions could be patched up using CFD for areas that did not have good paint coverage. Those distributions were then integrated to give forces and moments that provided corrections to the balance forces and moments in particular load and plume mass flow/pressure combinations that produced poor balance repeatability (caused by non-linear bellows behavior - fodder for another paper all together).

With a large number of configurations and AM/ACM variations to look at, the CFD tools were updated (not necessarily a validation in the purest sense) to closely match the experimental results and trends and to better represent the extrapolation to flight conditions and real solid rocket plumes. Because of subsequent change to the SLS as the launch vehicle, the normalized thrust levels tested no longer match the values expected in flight. Therefore the current database for ascent aborts is almost entirely based on CFD. The confidence gained through the collaborative testing and computations was critical to allowing this reliance on computed results for this potentially dangerous phase of flight. {Maybe put in a computed and measured pressure distribution if Jim has any published same as measured}

4.0 VALIDATION FOR UNSTEADY FLOWS

4.1 Transonic Capsule

While the need to understand the aerodynamics of most vehicles in a development environment mostly extends only to the time-averaged forces and moments, any significant separated flow will be unsteady. The Orion capsule descent aerodynamics were difficult to computed. The unsteadiness of the flow was one major culprit. Time-accurate computations of the flow helped a great deal but the details of the boundary layer state due to roughness was also a big driver. Relatively large uncertainty in the aerodynamic database below Mach

1 was not a particular problem, however CFD was used to estimate the opening loads of the drogue parachutes at M = 0.7 and this was of sufficient concern to make sure of the accuracy of the estimate.

Because of the unsteady nature of the flow, the unsteady aerodynamics had to be measured in order to properly verify the computations which also had to be time accurate. This experiment looked at the flow around a generic capsule of the same general proportions as the Orion capsule[25]. Figure 4-1 shows the model mounted in the wind tunnel on lateral struts to minimize the interference of the struts on the wake behind the capsule model. The laser light sheets for the PIV show the general areas of interest for the flow field measurements.

Since this was a dedicated CFD validation test, the test variations and instrumentation were specifically designed to measure important flow features. Of particular importance were the boundary-layer state on the heat shield, the unsteady pressures around the heat shield shoulder, and the unsteady and time-averaged wake flow. The angle of attack could be set to nominally 0°, 15°, and 30° and the Mach number ranged from 0.3 to 1.05. The heat shield was interchangeable - one smooth and one dimpled in a hexagonal pattern similar to a recessed texture of an Avcoat heat shield[26]. A close up photo of the rough heat shield is shown in Figure 4-2.

Measurements included time-averaged pressure using static taps and full-surface PSP, unsteady pressures around the heat-shield shoulder, time averaged and unsteady wake velocity, infrared (IR) imaging for transition detection, boundary-layer velocity distributions, and skin friction at the same location as the boundary-layer measurements. Figure 4-3 shows the instrumentation that was installed on the model.

Figure 4-4 shows where the wake measurements were made relative to the capsule. The wide-view wake images were captured at too slow a rate to get meaningful time histories of the large flow structures in the wake but with ~4,000 measurements, gave good mean and turbulence statistics. The smaller areas shown in the top view were sampled at 2,000 frames per second and provided a good look at the time history as well as statistical measures of turbulence and time-averaged velocity in that small region.

With so many unsteady and high-rate instruments involved in this test, the resulting data set is very large. That is one of the lessons from this test, the finer one has to look at a flow field for validating CFD, the more data required. The CFD for these unsteady, relatively high Reynolds number flows is also very data intensive. The PSP images in Figure 4-5 show the pressure coefficient on the model and model support at 3 different Mach numbers. The pressures are mapped onto a patched grid system containing a total of ~580,000 points in 89 structured grid blocks. While not a huge data set compared to what is contained in CFD results, it is quite dense compared to what is obtained from individual static taps.

An interesting aspect of this test was the ability of IR imagery to detect flow features other than boundary layer transition. Figure 4-6 shows some of the flow features for one test condition. The plastic material (3-D printed polycarbonate that was subsequently machined to an accurate final shape) helped maintain the small temperature differences between the areas of distinct flow regimes. In particular it was quite easy to image the suction peak on the shoulder on this model where with an aluminum or steel model, the heat conduction of the material smears the temperature differences making the flow features harder to discern.

Figure 4-7 shows two test points at Mach = 0.7 and Reynolds numbers of 1.3×10^6 and 10×10^6. Both are with the smooth heat shield. The low-Reynolds number condition shows laminar flow from attachment to separation while the higher-Re case shows transition wedges that were traced to small flaws in the surface, most of which were likely caused by particles in the flow striking the model (typically < 0.002" depth). A close up of Flaw #3 is shown Figure 3-8. The effect of boundary layer turbulence on the separation point is very clear in the figure since laminar and turbulent flow regions are side by side and the laminar flow separates immediately at the onset of an adverse pressure gradient while the turbulent flow continues around through significant pressure recovery before separating (Figure 4-5b).

The time-averaged velocity vectors in the wide-view PIV measurement plane are shown in Figure 4-9 with the color contours representing the x-velocity component. This was the primary information needed for determining the loads on the Orion drogue parachutes but is not sufficient to validate CFD tools. More information about the unsteady flow - beyond the rms values - is required to ensure that the computations are

accurate. The unsteady pressures, separation points, time variations in the wake structure all add to the picture of the flow for validation.

Figure 4-10 show an instantaneous velocity measurement in the smaller high-rate PIV measurement area. The instantaneous flow structure in Figure 4-10a looks completely different than the time-averaged flow in 4-10b. The rms x-velocity contours, Figure 4-10c, make sense in relation to the time-averaged flow structure with high levels in the shear layer and in the reverse-flow region.

4.2 Launch Vehicle Buffet

4.2.1 Space Launch System

Look up the SciTech ’16 papers and talk about validation implications. Maybe Cetin’s group published also?

4.2.2 Generic Hammerhead Launch Vehicle and Payload Fairing

The unsteady flow associated with bluff-body separation (or any separated flow) requires more data for validation. Not just time-accurate data but more data types in order to understand the important aspects of the flow. Another flow that is currently under study is the low-frequency buffet of launch vehicles. The study is not complete but will be published in the next few months but involves the flow over a hammerhead launch vehicle and payload fairing that was tested in 1962 by Coe and Nute[27]. In the case of buffet, it is important to understand the full picture of the time-varying pressures on the vehicle surface and to accurately integrate them to get the time-varying load. This is difficult to do in practice because the unsteady pressure sensors are relatively expensive and it is hard to install enough sensors to guarantee that the pressure integrations accurately represent the real forces. The approach has been to infer weighting factors based on the spatial coherence lengths associated with the flow at each of the sensors. The coherence lengths must be inferred from the individual sensor measurements so there is a bit of an art to measuring buffet forces.

The test was performed in order to determine the accuracy of the integrations typically performed for estimating buffet forces from sparse pressure data. Unsteady pressure data with high spatial density was acquired using unsteady PSP at sample rates of 5 kHz to 20 kHz to provide a data set that could be integrated

without coherence corrections and could be thinned out to look a the minimum density requirements and the accuracy of the coherence corrections for typical sparse instrumentation. The model is shown mounted in the 11- by 11-Foot Transonic Wind Tunnel at NASA Ames Research Center. ~210 unsteady pressure transducers were installed to verify the unsteady PSP response and for redundancy. Data records were approximately 8 seconds long when sampling at $_{m/s}$5 kHz. Data from this test will be published in January 2017 and it provides very detailed look at the unsteady pressures acting on this model at Mach numbers from 0.6 to 1.2.

5.0 CONCLUDING REMARKS

CFD validation testing comes in many forms and has been routine for decades often with little fanfare. Since aerodynamics projects generally include both experimental and CFD as tools for understanding doing them collaboratively provides much greater understanding of the problem being studied than either technique alone. Along with that understanding, the experimental data should provide clues as to strengths and weaknesses of the CFD tools. The CFD, when done early, provides valuable pre-test insight into both the problem being studied and how to improve the experiment. The highest return for generating aerodynamic databases, particularly for complicated geometries or flow conditions, has seemed to come from the inclusion of additional data acquisition during wind tunnel testing. This allows more confident use of CFD tools for filling in a database when the testing, for a variety of reasons, did not cover all the important flight conditions.

5.0 REFERENCES

[1] AIAA, "*Guide for the Verification and Validation of Computational Fluid Dynamics Simulations*," AIAA G-077-1998, 1998.

[2] Maskew, B., "Prediction of Subsonic Aerodynamic Characteristics – A Case for Low-Order Panel Methods," *Journal of Aircraft*, Vol. 19, No. 2, February 1982.

[3] Strash, D. J., Nathman, J. K., Maskew, B., and Dvorak, F. A., "Application of a Low-Order Panel Method – Program VSAERO – to Powerplant and Airframe Flow Simulations," AIAA paper 84-2178, AIAA 2nd Applied Aerodynamics Conference, August 1984, Seattle, WA.

[4] Körner, H., "Untersuchung zur Bestimmung der Druckverteilung an Flügel-Rumpf-Kombinationen Teil I: Messergebnisse fur Mitteldeckeranordnung aus dem 1,3-m Windkanal," DFVLR Bericht Nr. 0562, Braunschweig, 1969.

[5] Körner, H., "Untersuchung zur Bestimmung der Druckverteilung an Flügel-Rumpf-Kombinationen Teil II: Messergebnisse fur Mitteldeckeranordnung mit einem sehr dicken Rumpf, aus dem 1,3-m Windkanal," DFVLR Bericht Nr. 0611, Braunschweig, 1970.

[6] Körner, H., "Untersuchung zur Bestimmung der Druckverteilung an Flügel-Rumpf-Kombinationen Teil III: Messergebnisse fur Hoch- und Tiefdeckeranordnungen aus dem 1,3-m Windkanal," DFVLR Bericht Nr. 71/1, Braunschweig, 1971.

[7] Ross, J. C., Corsiglia, V. R., and Vogel, J. M., "Full-Scale Wind Tunnel Study of Wing-Fuselage Interaction and Comparison with Panel Methods", AIAA Aircraft Systems and Technology Meeting, Dayton, Ohio, August 11-13, 1981.

[8] Ashby, L. D., Dudley, M. D., Iguchi, S. K., Browne, L., and Katz, J., "Potential Flow Theory and Operation Guide for the Panel Code PMARC," NASA TM-102851, March 1990.

[9] Ross, J., Olson, L., Meyn, L., and Van Aken, J., "A New Design Concept for Indraft Wind-Tunnel Inlets with Application to the National Full-Scale Aerodynamics Complex," AIAA paper 1986-0043, 24th AIAA Aerospace Sciences Meeting, 1986.

[10] van Aken, J. M., Ross, J. C., and Zell, P. T., "Inlet Development for the NFAC 80- by 120-Foot Indraft Wind Tunnel", AIAA 6th Applied Aerodynamics Conference, June 6-8,1988, Williamsburg, Virginia, AIAA 88-2528.

[11] Olson, L. E., James, W. D., and McGowan, P. R., "Theoretical and Experimental Study of the Drag of Single- and Multi-Element Airfoils," *Journal of Aircraft*, Vol. 16, No. 7, July 1979, pp. 462-469.

[12] Storms, B. L., Takahashi, T. T., and Ross, J. C., "Aerodynamic Influence of a Finite-Span Flap on a Simple Wing," SAE Paper 95-1977, SAE Aerotech Conference, Sept. 18-21, 1995, Los Angeles, CA.

[13] Storms, B. L., Takahashi, T. T., and Ross, J. C., "Aerodynamics of a Simple Three-Dimensional High-Lift System," SAE Paper 96-1977, AIAA/SAE World Aviation Congress, Oct. 22-24, 1996, Los Angeles, CA.

[14] Mathias, D. L., Roth, K. R., Ross, J. C., Rogers, S. E., and Cummings, R. M., "Navier-Stokes Analysis of the Flow About a Flap Edge," *Journal of Aircraft*, Volume 35, No. 6, November-December 1998, pp. 833-838.

[15] Storms, B. L., et al, "An Aeroacoustic Study of an Unswept Wing with a Three-Dimensional High-Lift System," NASA TM-1998-112222, February 1998.

[16] McCallen, R. et al, "DOE's Effort to Reduce Truck Aerodynamic Drag – Joint Experiments and Computations Lead to Smart Design," AIAA paper 2004-2249, 34th AIAA Fluid Dynamics Conference and Exhibit, 2004.

[17] Heineck, J. T., Walker, S., Satran, D., "The Measurement of Wake and Gap Flows of a 1/8th Scale Generic Truck Using Three-Component Particle Image Velocimetry," *The Aerodynamics of Heavy Vehicles:* Trucks*, Buses and Trains*," edited by R. C. McCallen, F. Browand, and J. C. Ross, Lecture Notes in Applied and Computational Mechanics**,** Vol. 19, Springer-Verlag, Heidelberg, 2004.

[18] Ross, J. C. and Brauckmann, G. J., "Aerodynamic and Aeroacoustic Wind Tunnel Testing of the Orion Spacecraft," AIAA paper 2011-3160, 29th AIAA Applied Aerodynamics Conference, June 27-30, 2011, Honolulu, HI.

[19] Wolter, J. D., Childs, R., Wernet, M., Shestopalov, A., and Melton, J. E., "Flow Field Characterization of an Angled Supersonic Jet Near a Bluff Body," AIAA paer 2010-4829, 28th AIAA Applied Aerodynamics Conference, June 28 - July 1, 2010, Chicago, IL.

[20] Shestopalov, A. J., Childs, R. E., and Melton, J. E., "Turbulence Model Assessment for Hot Plumes," AIAA paper 2011-3340, 29th AIAA Applied Aerodynamics Conference, June 27-30,2011, Honolulu, HI.

[21] Brauckmann, G. J., Greathouse, J. S., and White, M. E., "Rocket Plume Scaling for Orion Wind Tunnel Testing," AIAA Paper 2011-3341, 29th AIAA Applied Aerodynamics Conference, June 27-30, 2011, Honolulu, HI.

[22] Childs, R. E., Garcia, J. A., Melton, J. E., Rogers, S. E., Shestopalov, A. J., and Vicker, D. J., "Overflow Simulation Guidelines for Orion Launch Abort Vehicle Aerodynamic Analyses," AIAA paper 2011-3163, 29th AIAA Applied Aerodynamics Conference, June 27-30, 2011, Honolulu, HI.

[23] McMullen, M. S., Childs, R. E., Stremel, P. M., Garcia, J. A., and Melton, J. E., "Validation of Computational Fluid Dynamics Analysis Methods on the Orion Launch Abort Vehicle," AIAA paper 2011-3162, 29th AIAA Applied Aerodynamics Conference, June 27-30, 2016, Honolulu, HI.

[24] Rogers, S. E. and Pulliam, T. H., "Computational Challenges in Simulating Powered Flight of the Orion Launch Abort Vehicle," AIAA paper 2011-3339, 29th AIAA Applied Aerodynamics Conference, June 27-30, 2011, Honolulu, HI.

[25] Ross, J. C., Heineck, J. T., Halcomb, N., Yamauchi, G. K., Garbeff, T., Burnside, N. J., Kushner, L. K., and Sellers, M., "Comprehensive Study of the Flow Around a Simplified Orion Capsule Model," AIAA paper 2013-2815, 31st AIAA Applied Aerodynamics Conference, June 24-27, 2013, San Diego, CA.

[26] Aluni, A. I., Olson, M. W., Gökcen, T., and Skokova, K. A., "Comparisons of Surface Roughness in Laminar and Turbulent Environments for Orion Thermal Protection System," AIAA paper 2011-3776, 42nd AIAA Thermophysics Conference, June 27-30, 2011, Honolulu, HI.

[27] Coe, C. F., and Nute, J. B., "Steady and Fluctuating Pressures at Transonic Speeds on Hammerhead Launch Vehicles," NASA TM-X-778, December 1962.

z

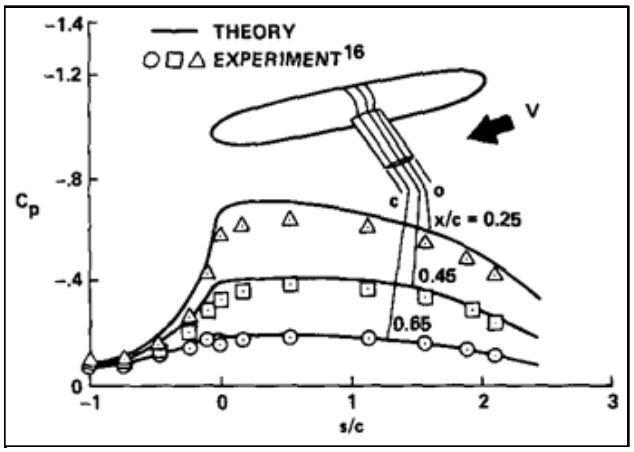

Figure 2-1: Span-wise pressure distribution from VASERO and wind tunnel. Symmetric airfoil and fuselage[4-6].

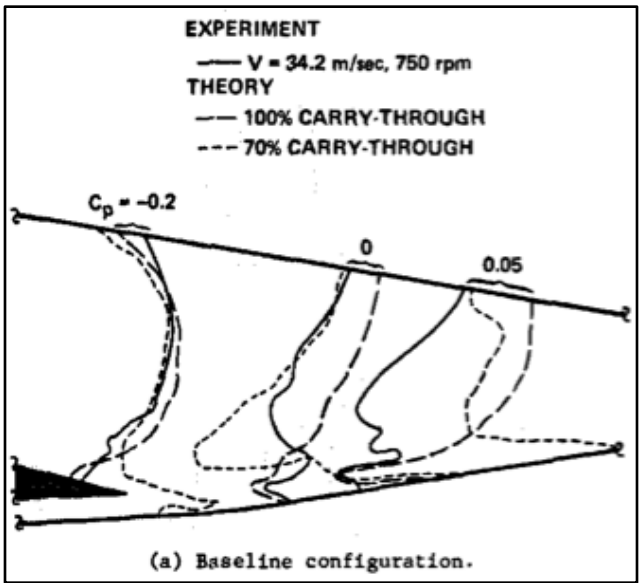

Figure 2-2: Fuselage pressure coefficient contours from Beech Sundowner experiment and VSAERO computations showing effect of fuselage carry-over lift modeling[7].

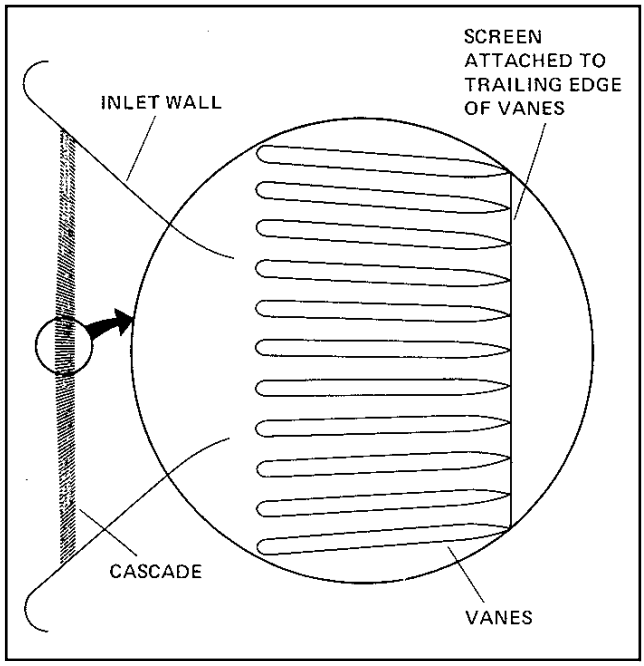

Figure 2-3: 2-D representation of 80- by 120-Foot Wind Tunnel inlet and its 120 vanes[9].

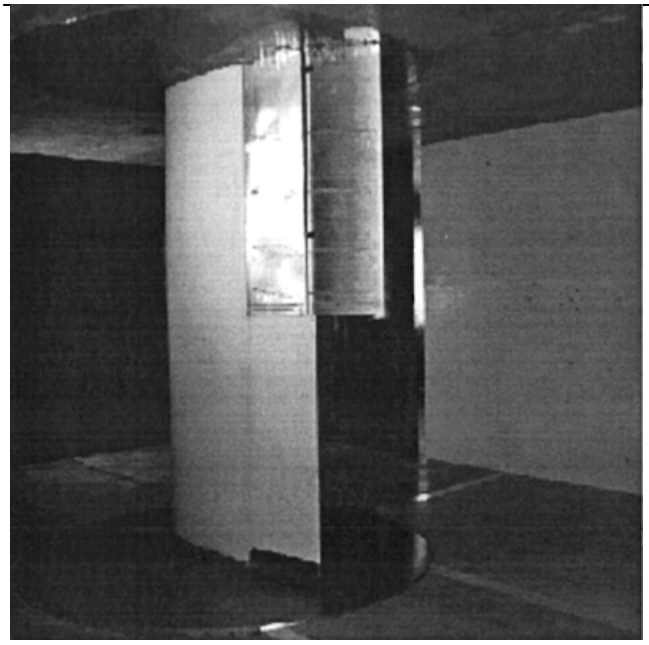

Figure 3-1: Part-span flap wing model in 7- by 10-Foot Wind Tunnel at NASA Ames Research Center.

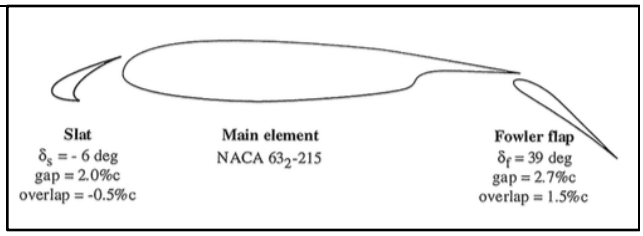

Figure 3-2: Three-component airfoil arrangement for the simple three-dimensional high-lift model[15].

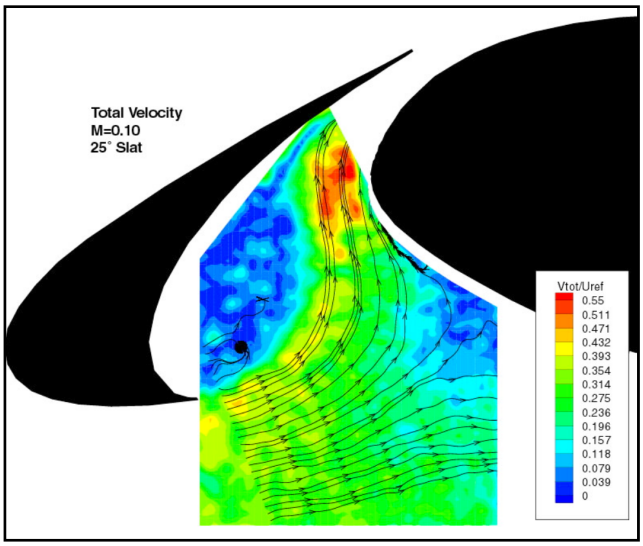

Figure 3-3: Two-component velocity measurements in slat cove of the simple three-dimensional high-lift model[15]. Mach number = 0.10, $\alpha = 10°$.

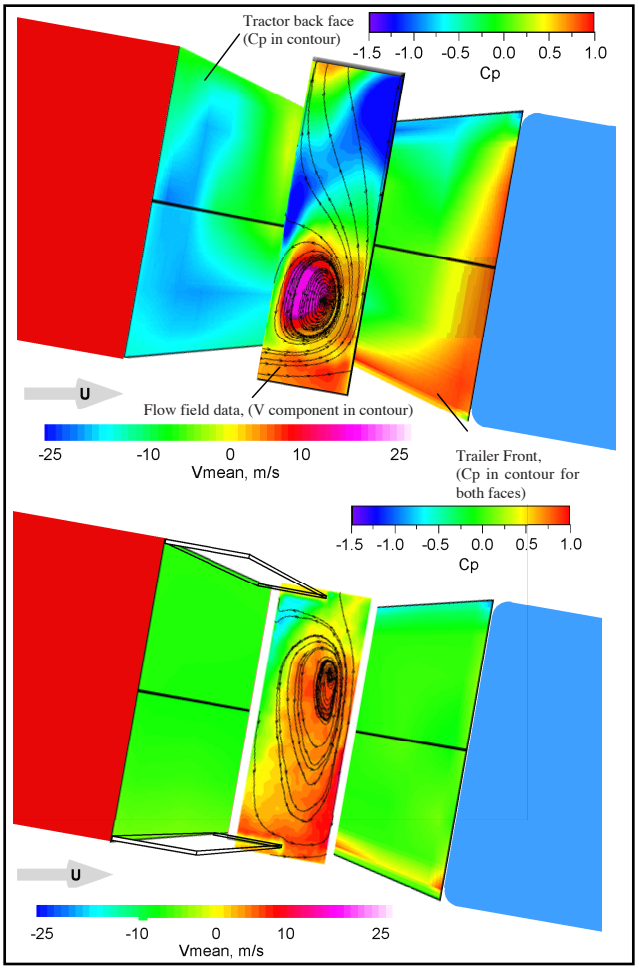

Figure 3-4: Composite illustrations of the surface pressures in the gap (without and with side extenders) and a flow field plot at 1/2 height. Surface pressure contours in Cp and flow field contour of the mean vertical velocity, in m/s [17].

Figure 3-5a: Boat tail plates on the back of a tractor trailer.

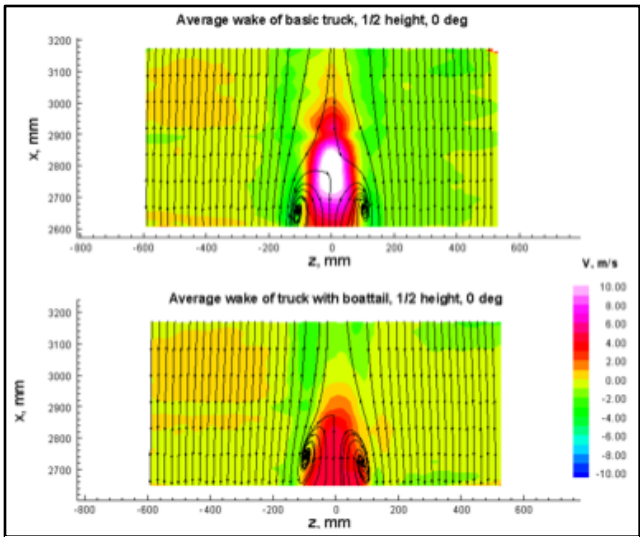

Figure 3-5b: Velocity measurements in the wake of a tractor/trailer with and without a boat-tail device. Streamlines show time-averaged velocity in a horizontal plane at 1/2 the trailer height. Color contours show the mean vertical velocity, in m/s [17]. Flow is from bottom to top.

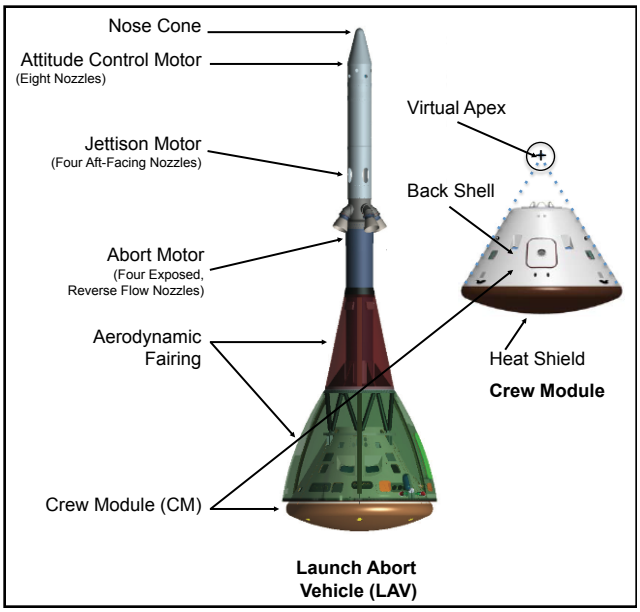

Figure 3-6: Components of the Orion spacecraft[18].

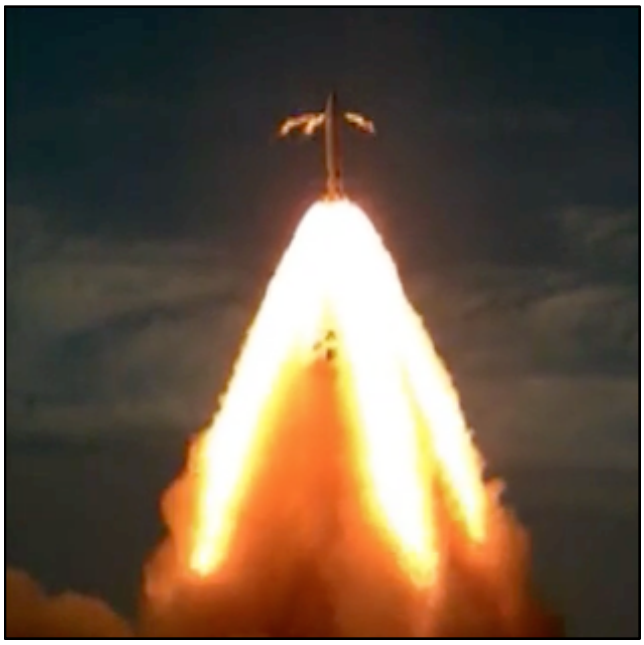

Figure 3-7: Abort and Attitude Control Motors firing during a pad abort test of the Orion[18].

Figure 3-8: Single AM nozzle with LAV body mounted downstream at NASA Glenn Research Center[19].

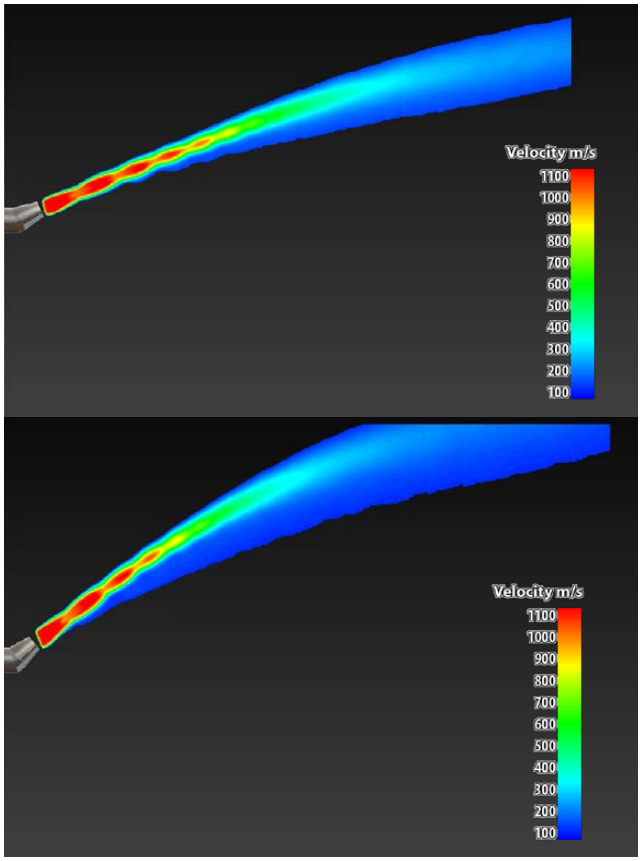

Figure 3-9: Velocity distribution measured in a plane bisecting the hot plume (~1350 R) measured using three-component PIV. 25° nozzle (top) and 40° nozzle (bottom). No LAV model for these data[18].

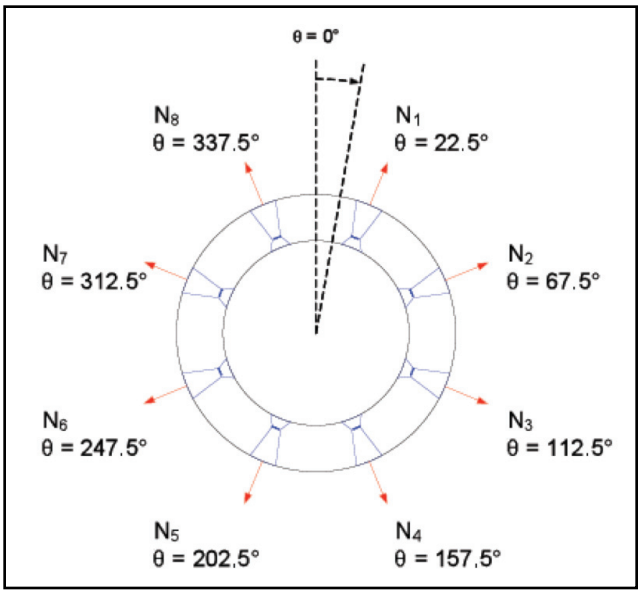

Figure 3-10: Section cut through the ACM nozzle array[18].

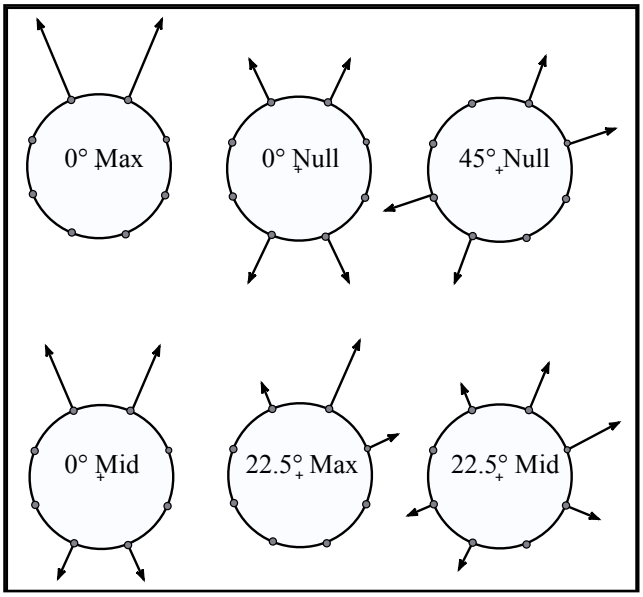

Figure 3-11: Examples of ACM firing direction and magnitude combinations[18].

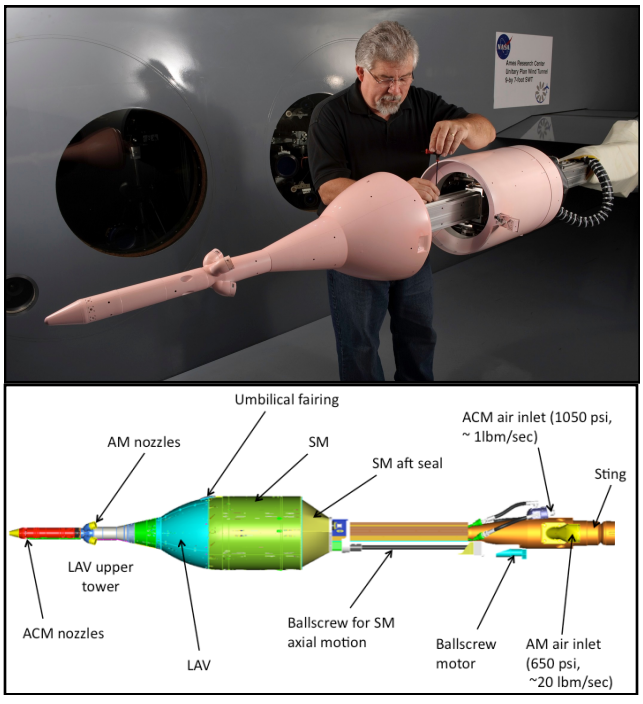

Figure 3-12: 6%-scale AM/ACM powered model in the 9x7 Foot Wind Tunnel at NASA's Ames Research Center (top) and CAD rendering (bottom) showing nozzle locations, high-pressure air supplies, and remotely positionable Service Module (SM)[18].

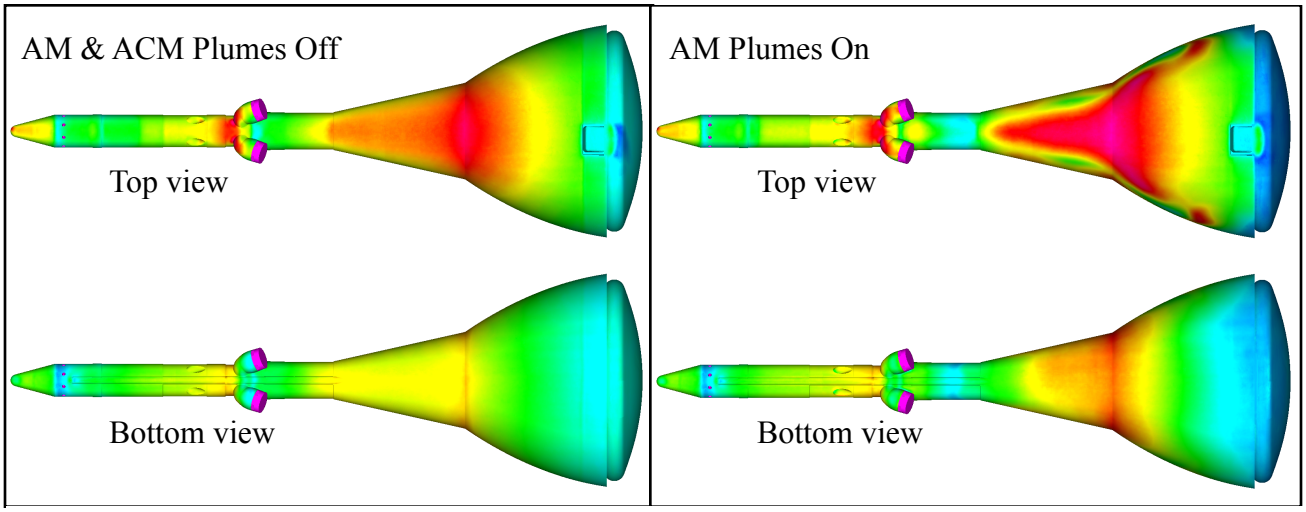

Figure 3-13: Example of PSP images from Orion powered LAV test. AM plumes off (left) and AM plumes on (right)[18].

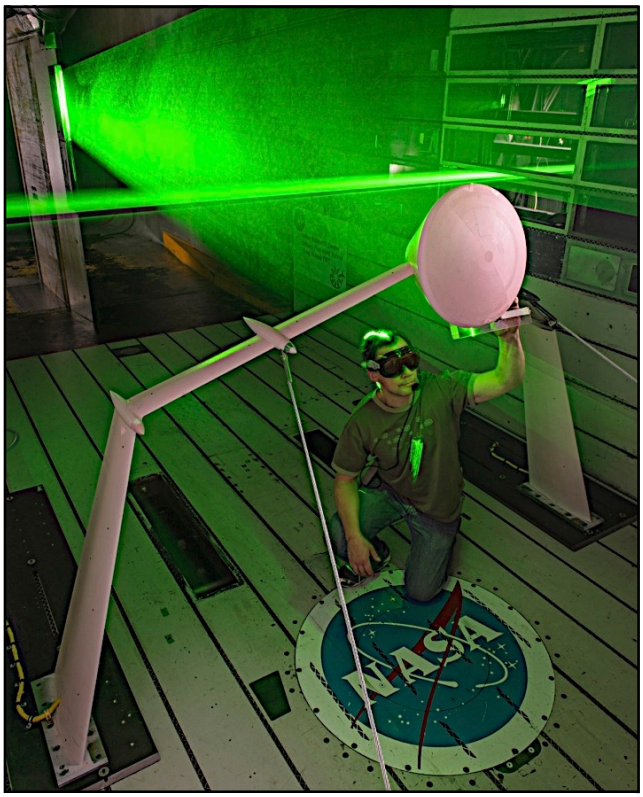

Figure 4-1: Capsule model mounted in the NASA Ames 11- by 11-Foot Transonic Wind Tunnel. PIV laser sheets show flow field measurement areas[25].

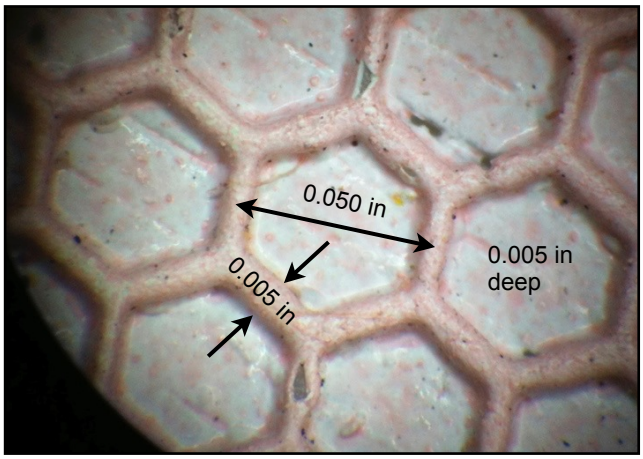

Figure 4-2: Simulated heat-shield roughness pattern machined into plastic heat shield. Pink is PSP on top of white base coat paint

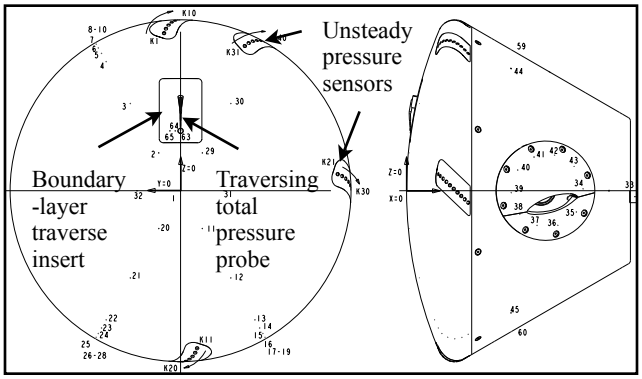

Figure 4-3: Capsule model showing location of instrumentation[25]. Unsteady pressure sensors at 4 locations around shoulder.

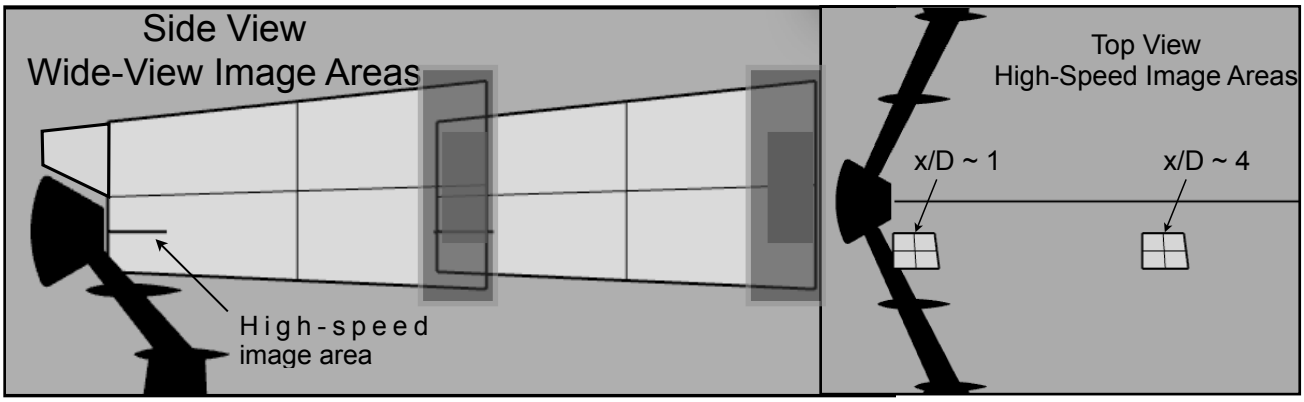

Figure 4-4: Locations of the PIV measurement areas relative to the capsule model in both positions in the test section. Greyed out are of the wide-view image areas were contaminated by wall reflections and the velocity could not be computed there[25].

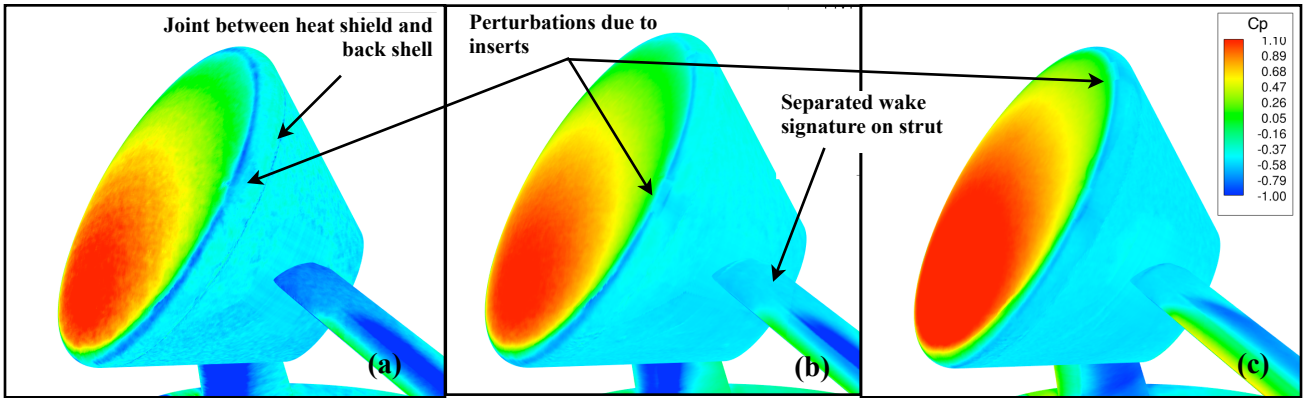

Figure 4-5: Effect of Mach number on heat shield pressure coefficient distribution at 15° angle of attack with the young heat shield: (a) M = 0.3, $Re_D = 5.3x10^6$; (b) M = 0.7, $Re_D = 10x10^6$; (c) M = 1.07, $Re_D = 7.3x10^6$[25].

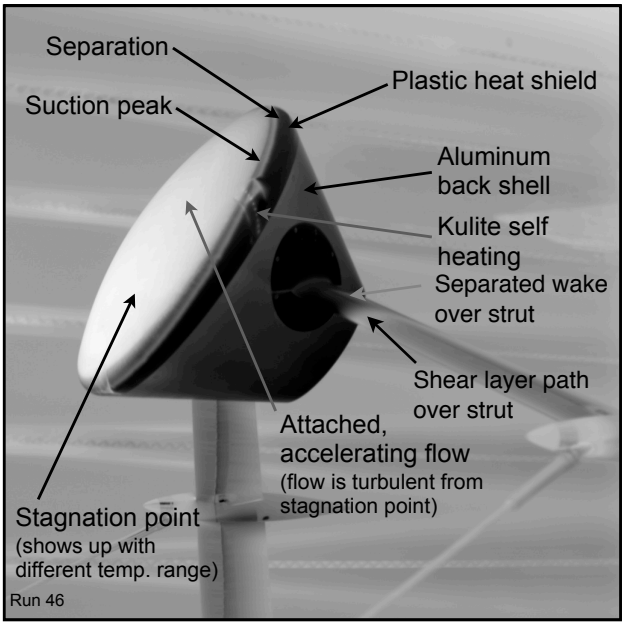

Figure 4-6: Flow features visible in IR images, Rough heat shield, M = 0.7, a = 30°, Re_D = $10x10^6$. Lighter areas are warmer[25].

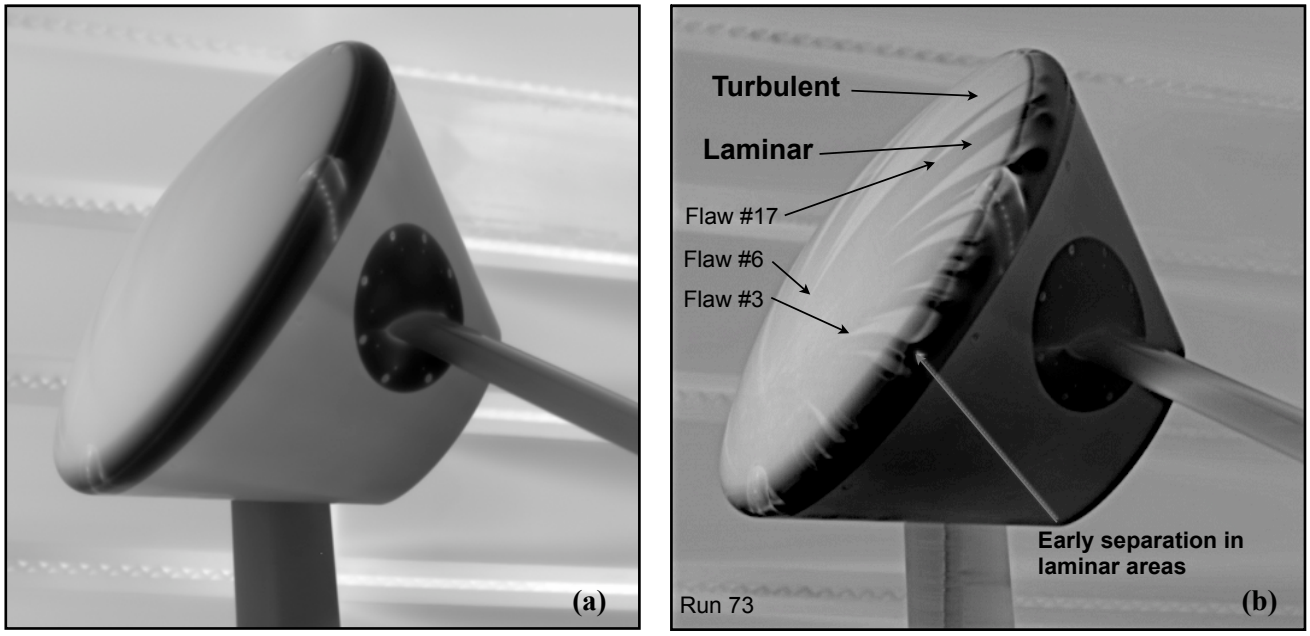

Figure 4-7: IR images of laminar and transitional flow on the smooth heat shield; M = 0.7, α = 30°: (a) $Re_D = 1.3x10^6$; (b) $Re_D = 10x10^6$[25].

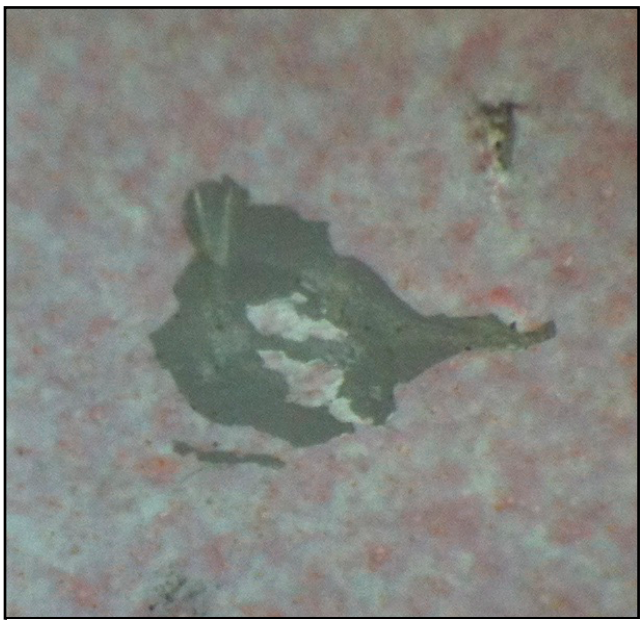

Figure 4-8: Flaw #3 from Figure 4-7.
Approximately 0.04” wide and 0.001” deep.

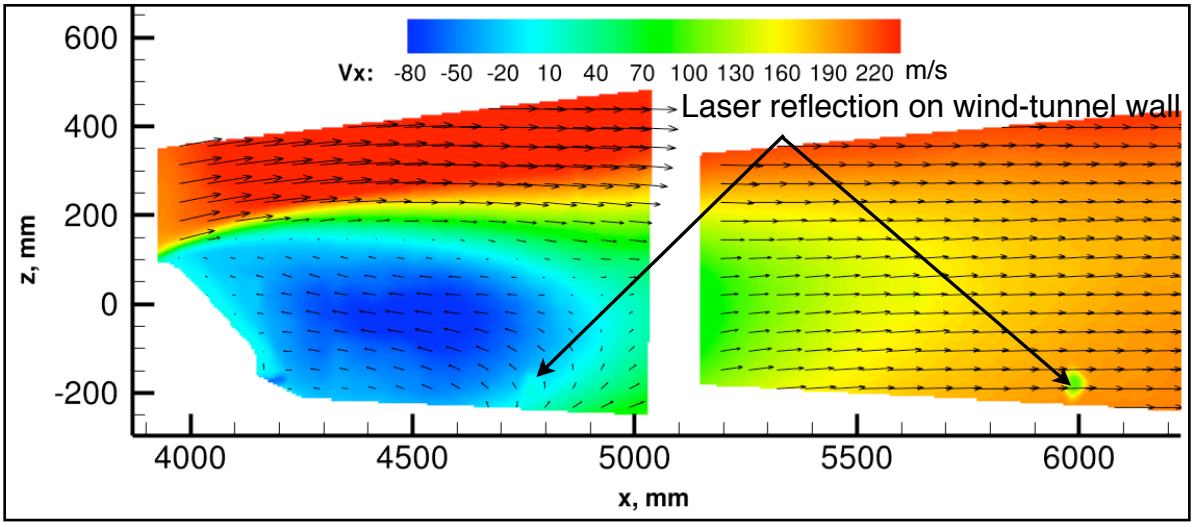

Figure 4-9: Average velocity in the capsule wake; M = 0.7, α = 14.0°, Re_D = 10x10^6. Velocity vectors in the plane; color contours represent x-component of velocity. Vectors have been

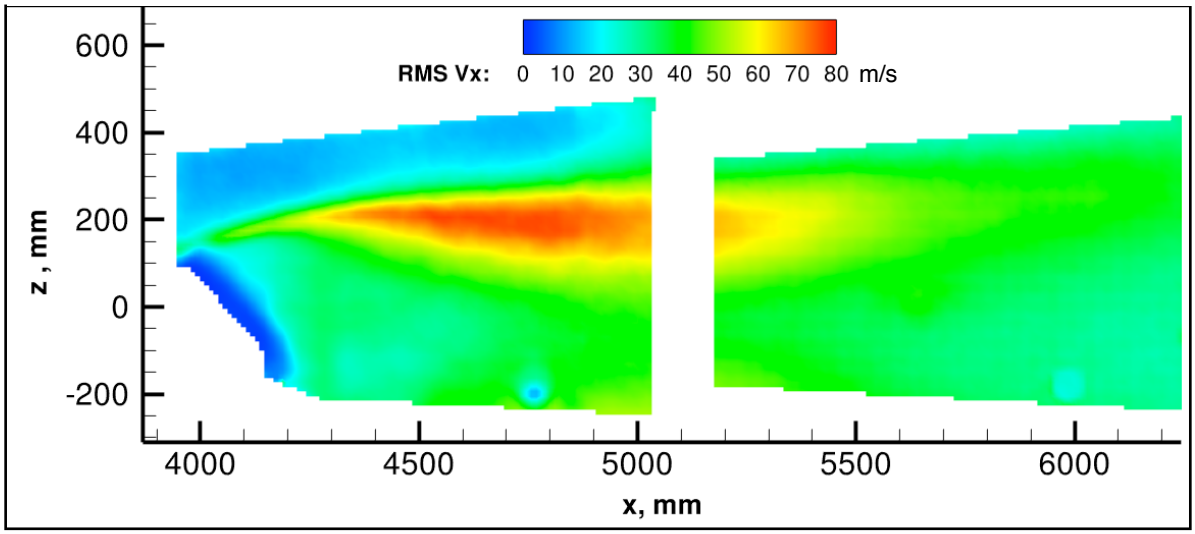

Figure 4-10: RMS x-velocity in capsule wake; M = 0.7, α = 14.0°, Re_D = 10x10^6[25].

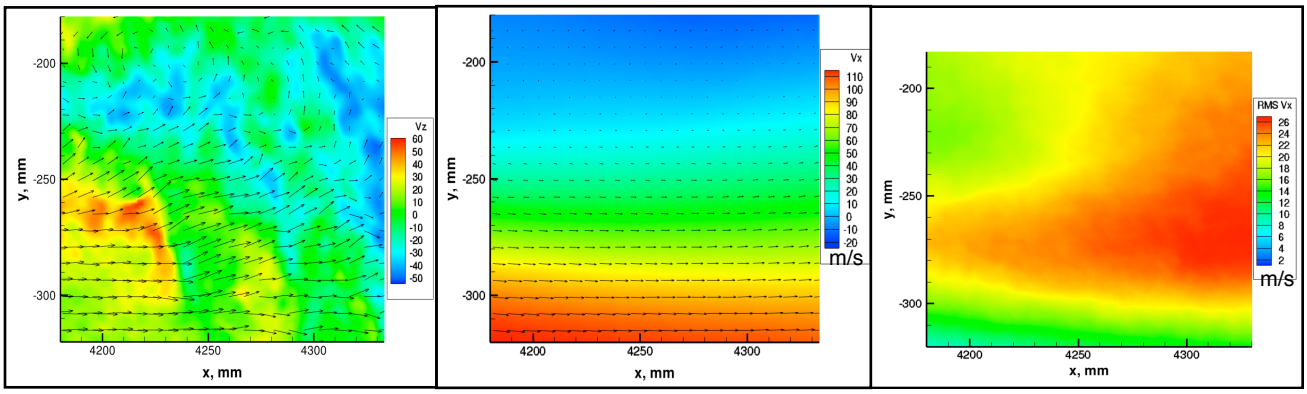

Figure 4-11: High-speed PIV measurements in capsule wake; M = 0.7, α = 14.0°, Re_D = 10x10^6 - (a) instantaneous velocity vectors and out-of-plane velocity contours; (b) time averaged velocity vectors and x-velocity component contours; (c) rms contours of x-velocity component[25].

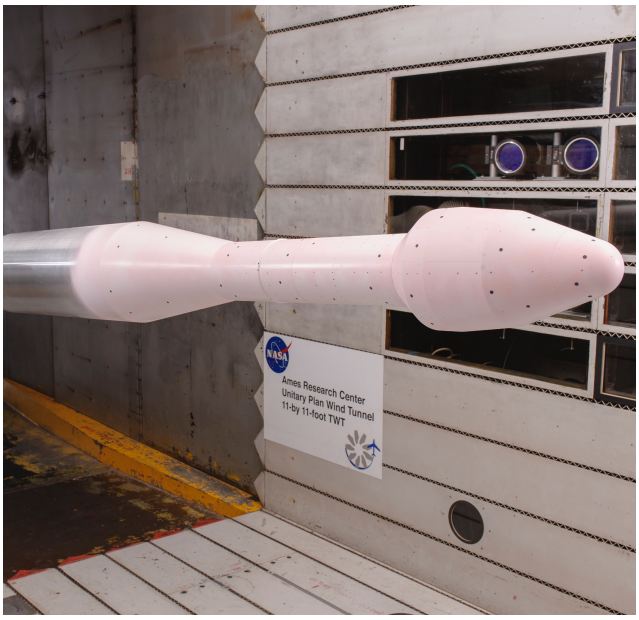

Figure 4-12: Generic hammerhead launch vehicle/ payload fairing model mounted in 11- by11-Foot Wind tunnel.